Wang, Z. X., Wang, Y. Q., Yun, X., Gardner, L. and Teh, H. L. (2021). Experimental study of swage-locking pinned aluminium alloy shear connections. Thin-Walled Structures, **(in press).**

Experimental study of swage-locking pinned aluminium alloy shear connections

Zhongxing Wang[a,b,c]*; Yuanqing Wang*[c]*; Xiang Yun*[d,e,f]*; *Leroy Gardner*[f]*; and Lip H. Teh*[g]

[a]*School of Civil Engineering, Tianjin University, Tianjin 300350, PR China*
[b]*Key Laboratory of Coast Civil Structure Safety of China Ministry of Education, Tianjin University, Tianjin 300072, PR China*
[c]*Department of Civil Engineering, Tsinghua University, Beijing 10084, PR China*
[d]*Department of Civil and Environmental Engineering, The Hong Kong Polytechnic University, Hong Kong*
[e]*Chinese National Engineering Research Centre for Steel Construction (Hong Kong Branch), The Hong Kong Polytechnic University, Hong Kong*
[f]*Department of Civil and Environmental Engineering, Imperial College London, London SW7 2AZ, UK*
[g]*School of Civil, Mining and Environmental Engineering, University of Wollongong, Wollongong 2500, Australia*

Abstract

This paper presents an experimental investigation into the structural behaviour and strength of swage-locking pinned aluminium alloy double-shear connections. It reports the failure modes (shear-out, bearing, block shear and net section failures), ultimate resistances and load-deformation histories. A total of twenty-three tests with four different aluminium alloy grades and various geometric variables, including end distances, edge distances and pin spacings, were carried out. The experimental results were utilized to assess the accuracy of the current American, Australian/New Zealand and European design provisions, as well as recent proposals by Teh and co-workers, extended to the design of aluminium alloy shear connections. The current code equations are shown to provide overly conservative strength predictions for the tested specimens. The equations of Teh and co-workers provide significantly more accurate strength predictions than the codes, though the test results indicate that there is still scope for more efficient design equations for swage-locking pinned aluminium alloy shear connections.

Keywords: Aluminium alloy; Shear connections; Swage-locking pin; Shear-out; Bearing failure; Net section rupture; Block shear.

1. Introduction

The past few decades have seen a significant increase in the structural applications of aluminium alloys in buildings and bridges, a selection of which is shown in Fig. 1: the Rafel Gallery (under construction) in Shanghai, featuring the largest aluminium alloy rooftop in the world (Fig. 1(a)), the Usnisa Palace in Nanjing, in which aluminium alloy members with large cross-sectional sizes were used to form a spatial reticulated dome structure [1] (Fig. 1(b)), the Howard Auditorium in Tulsa featuring a Buckminster Fuller style, aluminium alloy geodesic dome [2] (Fig. 1(c)) and an 88-m span arch bridge over Saguenay River in Arvida, which was the first (constructed in 1950 and still remaining in service) all-aluminium highway bridge in North America [3] (Fig. 1(d)).

Considerable research has been conducted on the structural performance of aluminium alloy members, covering local and global buckling behaviour of beams [4,5], columns [6,7] and beam-columns [8,9]. The research has demonstrated that the structural performance of aluminium alloy members is quite different from that of structural steel members, owing primarily to the distinct stress-strain behaviour of aluminium alloys. However, far less research has been carried out into the strength of aluminium alloy connections, which play a crucial role in the performance of framed structures.

Since the weldability of commonly used aluminium alloys in construction, such as 6061-T6 and 6063-T5, is poor, fastener connections are more extensively used to join aluminium elements. Menzemer et al. [10] carried out a series of tests on single-shear connections made of three kinds of aluminium alloys, with the aim to understand the influence of sheet confinement and bolt preload on the bearing strength of the shear connection. Tajeuna et al. [11] performed tests on bolted single and double shear connections between structural steel and aluminium alloy 6061-T6, complemented with finite element analyses, to investigate the effect of certain geometric parameters on the strength of the connections. Cho and Kim [12] carried out experimental and numerical investigations into the structural behaviour of bolted single-shear connections, and proposed a new design method considering the effective shear stress in a block shear failure and the curling effect. A similar investigation [13] was performed on connections made of a higher strength aluminium alloy (7075-T6). Wang et al. [14] tested aluminium alloy bolted connections, performed a comprehensive numerical study, and proposed a new design method capable of accurately predicting the bolt shear force in long joints.

The employment of conventional bolted connections in aluminium structures, however, involves several important issues, such as self-loosening [15,16], electrochemical corrosion of aluminium alloy plates if connected by ordinary steel bolts [19] and thread galling of stainless steel bolts [20,21]. With advances in fastener manufacturing, a novel category of fasteners – swage-locking pins (also referred to lockbolts) [17,18] has been developed and is now being increasingly applied in aluminium alloy structures [22-24]. For example, the fasteners used in the Rafel Gallery, shown in Fig. 1(a), are swage-locking pins. The present paper investigates the structural behaviour and strength of swage-locking pinned shear connections in four different aluminium alloys.

A total of twenty three double-shear connections with a single swage-locking pin (CS), double swage-locking pins arranged transversely to the loading direction (CDT), or double swage-locking pins arranged in the loading direction (CDL), were tested. The test results are used to evaluate the accuracy of the design equations specified in the current Aluminium Design Manual (AA 2015) [25], Australian/New Zealand standard for aluminium structures (AS/NZS 1664.1:1997) [26] and EN 1999-1-1:2007 (EC9) [27], as well as the equations proposed by Teh and co-workers [28-32].

2. Experimental programme

2.1 Tension coupon tests

Twelve tension coupons extracted from the aluminium alloy plates used to form the connection test specimens were tested to determine the material stress-strain response of the four investigated aluminium alloys − 6061-T6, 6063-T5, 6082-T6 and 7A04-T6. The dimensions of the tensile coupons, which complied with the requirements given in ASTM E8M-15 [33], are given in Fig. 2(a). For each aluminium alloy, three coupon tests were conducted. Displacement control was adopted in a 300-kN hydraulic testing machine at a constant rate of 1.0 mm/min (the same loading rate as used for the testing of shear connections).

The measured stress-strain curves of the four aluminium alloys are shown in Fig. 2, together with the curves fitted using the Ramberg-Osgood (R-O) model [34]; a more accurate two-stage Ramberg-Osgood model has recently been proposed for aluminium alloys [35]. The measured material properties are summarised in Table 1, where E is the Young's modulus, $f_{0.2}$ is the 0.2% proof stress, f_u is the ultimate stress, n is the exponent used in the R-O constitutive model, ε_u is the strain at the ultimate stress and ε_f is the fracture strain. Note that the fracture strains were determined based on (1) elongation $\varepsilon_{f,el}$ and (2) area reduction $\varepsilon_{f,re}$, as given by Eqs. (1) and (2), respectively:

$$\varepsilon_{f,el} = \ln\left(L_f / L_0\right) \tag{1}$$

$$\varepsilon_{\mathrm{f,re}} = \ln\left(A_0 / A_{\mathrm{f}}\right) \tag{2}$$

in which L_0 and A_0 are respectively the original gauge length and cross-sectional area of the coupons, L_f is the gauge length after fracture, and A_f is the cross-sectional area of the fracture surface, which was calculated as the product of the measured width and thickness at the fractured cross-section. In ductile materials, fracture takes place in a region of increasingly concentrated plastic strains following localized necking. Fracture strain determined based on elongation $\varepsilon_{f,el}$ suffers from being gauge length dependent (50 mm was chosen herein) [36], whereas fracture strain calculated based on area reduction $\varepsilon_{f,re}$ at the fracture surface does not encounter this drawback. As shown in Table 1, the measured values of $\varepsilon_{f,re}$ are substantially higher than the corresponding values of $\varepsilon_{f,el}$. It can also be observed that the ductility of the aluminium alloys decreases significantly with the increase in tensile strength.

2.2 Specimens, rig and operation of the shear connection tests

A total of twenty three tests were conducted to investigate the structural behaviour and strength of swage-locking pinned aluminium alloy double-shear connections. The effects of key variables, including the aluminium alloy grade, the end distance (e_1), the edge distance (e_2), the pitch (p_1) and the gauge distance (p_2), on the connection strength were investigated. The geometric variables are defined in Fig. 3. The failure of each shear connection was designed to occur in the aluminium alloy plates. Note that the present study is focussed on the swage-locking pinned aluminium alloy shear connections with failure in the connected plates, while the mechanical properties and resistances of the swage-locking pins have been studied by Wang et al. [24].

The tested connections included three different pin configurations – connections with a single swage-locking pin (CS), connections with double swage-locking pins arranged transversely to the loading direction (CDT) and connections with double swage-locking pins arranged in the loading direction (CDL), as shown in Fig. 3. The nominal thicknesses of the inner and the outer plates are 4 and 12 mm, respectively, for all specimens. The nominal diameter of the pin (d_{pin}) is 9.66 mm and the nominal diameter of the hole (d_0) is 10.5 mm. The detailed information of the test specimens, including the connection type, specimen label, aluminium alloy grade and geometric dimensions, are summarised in Table 2. Note that the nominal geometric dimensions of the plates and pins were confirmed by measurement and found to be very accurate and consistent; hence, the measured dimensions are taken to be the same as the nominal values.

The test specimens are labelled such that the connection type (CS, CDT or CDL), aluminium alloy grade (6061-T6, 6063-T5, 6082-T6 or 7A04-T6), end distance (10, 15, 20, 30 or 40 mm), edge distance (10, 15, 20, 30, 40 or 50 mm) and pin spacing (20, 25, 30 or 40 mm) can be clearly identified. For the CS specimens, the pin spacing is not included in the labelling system, while for the CDT and CDL specimens, the last number in their labels represents either the gauge distance (p_2) or the pitch (p_1), respectively. For example, the label CDT-61-30-10-40 indicates a CDT specimen made of 6061-T6 aluminium alloy with an end distance of 30 mm, an edge distance of 10 mm and a gauge distance of 40 mm.

The clearance between the hole and the pin shank was eliminated before conducting the shear connection tests. The shear connections tests were conducted in a WE-100B hydraulic testing machine with a maximum loading capacity of 100 kN, as shown in Fig. 4. The tests were carried out under displacement control at the same rate (1 mm/min) as that used for the tension coupon tests, thus enabling the material properties of the components of the shear connections to be, as far as possible, similar to those obtained from the tension coupon tests [28]. The ends of the inner plates were tightly gripped in the jaws of the testing machine, ensuring that the test specimens remained vertical (i.e. avoiding in-plane rotation) [37].

The displacements at selected positions were captured by means of a video gauge (model: iMETRUM); the measurement points were marked onto the edges of the inner (see Points U1 and D1 in Fig. 3(a)) and outer (see Points L1, L2, R1 and R2 in Fig. 3(a)) plates. The applied load and the displacements at the measurement points were recorded using two data loggers, operating at the same frequency.

3. Results of shear connection tests and comparisons with design methods

3.1 Failure modes

Four failure modes − shear-out (SO, also termed end tear-out), bearing (B), net section (NS) and block shear (BS) failures − were observed in the tests. Failure modes of all specimens are shown in Figs. 5-7 and summarised in Table 3.

It can be seen from Fig. 5 that the threshold value of e_1 between bearing and shear-out failures is about 3.11 (=30/9.66) times the pin diameter, as Specimen CS-61-30-50 exhibited a barely discernible shear-out deformation. The fact that the 6061-T6 aluminium specimen failed in shear-out is evident from the load-displacement curves shown in Fig. 8(a), which reveal that the CS specimens with end distances e_1 ranging from 10 to 30 mm (which failed in shear-out) had a precipitous drop in their load-carrying capacity, in contrast to Specimen CS-61-**40**-50 (which failed in bearing). The experimentally indicated threshold is almost the same as the value of 3.17 derived by Teh and Uz for bolted steel connections [29].

Fracture transverse to the loading direction took place at the side (flank) of the pin hole in Specimen CS-04-15-50; this could have been due to the presence of a crack or other defect. It is also noted that the ultimate test load is somewhat lower than the estimate obtained using the shear-out equation proposed by Teh and Uz [30], as shown in Table 3.

Figure 6 shows that the CDT specimens with widths less than 80 mm failed by net section rupture, while the wider specimens failed by block shear. However, the gauge distance p_2 had no effect on the failure modes of the tested CDT specimens.

As shown in Fig. 7, the downstream pin of each CDL specimen failed with barely any discernible shear-out deformation as the end distance e_1 was almost the same as the identified threshold value between shear-out and bearing failure (see the second paragraph of this section), consistent with Specimen CS-61-30-50. However, the upstream pin of the specimens with pitches up to 30 mm failed in shear-out, as evident from the photographs showing shear failure planes between the upstream and the downstream pins. Note that the threshold value for the pitch p_1 was found by Teh and Uz to be equal to 3.42 times the pin diameter [29], 8% longer than that for the end distance e_1. The first three specimens shown in Fig. 7 can therefore be treated as having failed in combined bearing and shear-out in computing their resistance, while Specimen CDL-61-30-50-40 is treated as having failed in bearing.

3.2 Ultimate loads and load-deformation responses

The experimentally obtained ultimate loads (P_t) are summarised in Table 3, and are plotted in Figs. 8-10 against the corresponding average deformation (e_h) of the inner aluminium alloy plates, calculated from Eq. (3),

$$e_h = \frac{1}{2}\left(\frac{(d_{U1}-d_{L1})+(d_{U1}-d_{R1})}{2}+\frac{(d_{L2}-d_{D1})+(d_{R2}-d_{D1})}{2}\right) \quad (3)$$

in which d_{U1}, d_{D1}, d_{L1} and d_{R1} are the measured displacements at gauge points U1, D1, L1 and R1 (see Fig. 3(a)), respectively.

Figure 8 shows that the specimens made of 6063-T5 aluminium alloy exhibited the best deformation capacity among the tested specimens. The load-carrying capacities of the 6063-T5 specimens did not drop so precipitously as the other specimens, especially in bearing failures where the shear stresses could be redistributed downstream as fracture propagated from the critical zones adjacent to the pin holes.

As can be seen from Fig. 9(a), failure of the net section between the pin holes (i.e. the inner net section) did not always take place at the same time as failure of the net section flanking the pin holes (i.e. the outer net section). If the edge distance e_2 is very small relative to the gauge distance p_2, the outer net section may fracture well before the inner section due to the different level of shear lag in the inner and outer net sections [28]. However, it can be inferred from the presence of a plateau (rather than a rising curve) following the drop after the ultimate load point that the inner net section of these specimens was already at the ultimate stress (f_u) when the ultimate load was reached.

For specimens failing in block shear, a plateau region was also observed after the precipitous drop from the ultimate load, as shown in Fig. 9(b). The shear failure took place well after the complete tensile failure of the inner net section, and the plateau region indicates the resistance provided by the shear area. Similar load resistances were obtained at the plateau region of Specimens CDT-61-30-40-20, CDT-61-30-40-25 and CDT-61-30-40-30 due to their same effective shear area (as detailed in the following sub-section). The very low shear resistance following the tensile failure of Specimen CDT-61-30-40-40, which had the same shear area, suggests that some shear fracture had taken place prior to the precipitous drop in the load-carrying capacity. It can be observed from Fig. 10 that the CDL specimens with pitches less than 30 mm (which failed in shear out) showed reduced ductility relative to those with greater pitches (Specimens CDL-61-30-50-30 and CDL-61-30-50-40); the lower ductility of Specimens CDL-61-30-50-20 and CDL-61-30-50-25 resulted from the premature shear-out failure at their upstream pin holes. However, there were some inconsistencies in the relationship between the achieved ductility and the pitch, most likely due to the variability in frictional resistance.

3.3 Comparisons with codified design provisions

Existing design rules for aluminium alloy shear connections set out in the American aluminium design manual (AA 2015) [25], Australian/New Zealand standard for aluminium structures (AS/NZS 1664.1:1997) [26] and EN 1999-1-1:2007 (EC9) [27] are evaluated in this sub-section by comparing the predicted design resistances with the obtained test results, as presented in Table 3. The ultimate test load is denoted P_{Test}, while P_{AA}, $P_{\mathrm{AS/NZS}}$ and P_{EC9} are the nominal design resistances calculated according to AA [25], AS/NZS 1664.1:1997 [26] and

EC9 [27], respectively. In all comparisons, the measured geometric and material properties have been used and all partial safety factors have been set to unity.

Note that in the three design specifications, shear-out is generally treated as a special case of bearing failure, and thus both the bearing and shear-out resistances are denoted as P_B in this sub-section. The predicted design resistance is taken as the lowest value among the bearing (or shear-out) (P_B), net section (P_{NS}) and block shear (P_{BS}) resistances.

3.3.1 Code bearing and shear-out resistances (P_B)

The design equation for calculating the bearing and shear-out resistances $P_{B,AA}$ of each bolt according to AA 2015 [25] is given by Eq. (4),

$$P_{B,AA} = e_1 t f_u \leq 2 d_{pin} t f_u \quad (4)$$

in which t is the thickness of the inner plate.

The bearing and shear-out design resistances $P_{B,AS/NZS}$ specified in AS/NZS 1664.1:1997 [26] is quite similar to that set out in AA 2015 [25], as given by Eq. (5),

$$P_{B,AS/NZS} = 2 d_{pin} t f_B \quad (5)$$

where f_B is the bearing stress, which can be calculated from Eq. (6):

$$f_B = \begin{cases} \min\left(f_{0.2}, \dfrac{f_u}{1.2}\right) & \text{for } e_1 \geq 2d_{pin} \\ \dfrac{e_1}{2d_{pin}} \min\left(f_{0.2}, \dfrac{f_u}{1.2}\right) & \text{for } e_1 < 2d_{pin} \end{cases} \tag{6}$$

The current EC9 [27] expression for calculating the bearing and shear-out resistances $P_{B,EC9}$ of aluminium alloy connections is the same as that used for structural steels (EN 1993-1-8) [38], as given by Eq. (7),

$$P_{B,EC9} = k_1 \alpha_b f_u dt \text{, with } \alpha_b = \min\left(\alpha_d, \frac{f_{up}}{f_u}, 1.0\right) \tag{7}$$

where $\alpha_d = e_1/3d_0$ for end pins and $\alpha_d = (p_1/3d_0 - 0.25)$ for inner (upstream) pins, d_0 is the diameter of the pin holes, f_{up} is the ultimate stress of the pin material and k_1 is a parameter considering the influence of edge distance and gauge distance, which can be calculated from Eq. (8):

$$k_1 = \begin{cases} \min\left(2.8\dfrac{e_2}{d_0} - 1.7, 2.5\right) & \text{for edge pins} \\ \min\left(1.4\dfrac{p_2}{d_0} - 1.7, 2.5\right) & \text{for inner pins} \end{cases} \tag{8}$$

For the specimens connected by more than one pin, the bearing and shear-out resistances are calculated as the sum of the resistances of the individual pins according to the respective specifications. Note that e_1 should be replaced by ($p_1 – d_0/2$) (i.e. the distance from the centre of the upstream pin hole to the edge of the downstream pin hole) when using Eqs. (4)-(6) to calculate the bearing or shear-out resistance of the upstream pin of the CDL specimens.

3.3.2 Code net section tension resistance (P_{NS})

According to AA 2015 [25] and AS/NZS 1664.1:1997 [26], the net section tension resistance ($P_{NS,AA}$ or $P_{NS,AS/NZS}$) is simply the product of the net tension area of the critical plate at the section containing the pin holes A_n and the plate ultimate stress f_u, as given by Eq. (9). In EC9 [27], a reduction factor of 0.9 is applied for the calculation of the net section tension resistance $P_{NS,EC9}$, as given by Eq. (10).

$$P_{\mathrm{NS,AA}} = P_{\mathrm{NS,AS/NZS}} = A_{\mathrm{n}} f_{\mathrm{u}} \tag{9}$$

$$P_{\mathrm{NS,EC9}} = 0.9 A_{\mathrm{n}} f_{\mathrm{u}} \tag{10}$$

3.3.3 Code block shear resistance (P_{BS})

AA 2015 [25] determines the block shear resistance (see Fig. 11) $P_{BS,AA}$ based on the relationship between the net area in shear (A_{nv}) and the net area in tension (A_{nt}), as given by Eqs. (11a) and (11b),

$$\text{For } A_{nt} \geq 0.6\,A_{nv}\text{: } P_{BS,AA} = f_{vy}A_{gv} + f_uA_{nt} \tag{11a}$$

$$\text{For } A_{nt} < 0.6\,A_{nv}\text{: } P_{BS,AA} = f_{vu}A_{nv} + f_{0.2}A_{gt} \tag{11b}$$

where A_{gv} and A_{gt} are the gross shear and the gross tensile areas, respectively, f_{vy} is the yield stress in shear taken equal to $0.6f_{0.2}$ and f_{vu} is the ultimate shear stress taken as $0.6f_u$.

Eq. (11a) represents block shear failure as rupture of the net tensile area and yielding of the gross shear area, while Eq. (11b) assumes block shear failure to be caused by rupture of the net shear area and yielding of the gross tensile area. However, there is no particular technical basis for either mechanism, as explained by Teh & Deierlein [32].

The design block shear resistance $P_{BS,EC9}$ according to EC9 [27] is calculated based on yielding of the net shear area and rupture of the net tensile area, as given by Eq. (12).

$$P_{BS,EC9} = \frac{\sqrt{3}}{3} f_{0.2}A_{nv} + f_uA_{nt} \tag{12}$$

EC9 adopts the von Mises shear coefficient of $\sqrt{3}/3$ rather than the simplified shear coefficient of 0.6 employed in AA 2015. No design expression for block shear resistance is given in AS/NZS 1664.1:1997 [26], hence the block shear failure is not accounted in the calculations of $P_{AS/NZS}$.

3.3.4 Summary of code results

As indicated in Tables 3 and 4, the three codified design methods [25-27] yield very conservative resistance predictions for the tested specimens, with the mean values of P_{Test}/P_{AA}, $P_{Test}/P_{AS/NZS}$ and P_{Test}/P_{EC9} being 1.50, 1.82 and 1.53, respectively. The design resistances of almost all tested connections are governed by the bearing (shear-out) failure mode due to the unduly conservative bearing (shear-out) equations, with only three specimens (CDT-61-30-40-20, CDT-61-30-40-25 and CDT-61-30-40-30) governed by the block shear mode according to EC9 [27].

It can be observed from Table 3 that the code equations yield the most conservative predictions for the connections made of 6063-T5 aluminium alloy, which exhibits the most ductile behaviour. For the specimens made of high strength aluminium alloy 7A04-T6, conservatism is also generally present in all the design predictions, but to a much lesser extent.

The design resistances based on the experimentally observed failure modes are also compared with the ultimate test loads, as shown in Table 5. Owing to the similarity of the design approaches in AA 2015 [25] and AS/NZS 1664.1:1997 [26], the latter is not included in Table 5. It is clear from Table 5 that the current code bearing (and shear-out) equations are the most conservative by far, even if consideration is given to the possible contribution of the friction forces between the inner and the outer plates.

3.4 Comparisons with design equations proposed by Teh et al.

Teh and co-workers [28-32,37] proposed a number of equations for predicting the resistances of bolted shear connections made of structural cold-reduced or hot-rolled steel, which have been shown to yield better accuracy than the current code equations. Their equations have been included in AISI S100-16 [41] and AS/NZS 4600:2018 [42], and are expected to be incorporated into the next version of the Aluminium Design Manual 2020. In this section, the accuracy of their equations for the design of aluminium alloy shear connections is evaluated through comparisons of the ultimate test loads P_{Test} with the predicted resistances P_{Teh}, as shown in Table 3.

The value of P_{Teh} for each specimen is taken as the lowest among the predicted shear out resistance $P_{\mathrm{SO,Teh}}$, bearing resistance $P_{\mathrm{B,Teh}}$, net section tension resistance $P_{\mathrm{NS,Teh}}$ and block-shear resistance $P_{\mathrm{BS,Teh}}$. The lowest value of $P_{\mathrm{SO,Teh}}$, $P_{\mathrm{B,Teh}}$, $P_{\mathrm{NS,Teh}}$ and $P_{\mathrm{BS,Teh}}$ defines the predicted failure mode, denoted $\mathrm{FM}_{\mathrm{Teh}}$ in Table 4. The design equations proposed by Teh and co-workers [28-32] are described in the following sub-sections.

3.4.1 Shear-out resistance ($P_{\mathrm{SO,Teh}}$)

Teh and Uz [30] proposed Eq. (13) for the shear-out resistance of structural-steel bolted connections:

$$P_{\mathrm{SO,Teh}} = 1.2 L_{\mathrm{av}} t f_{\mathrm{u}} \tag{13}$$

in which L_{av} is the active shear length equal to ($e_1 - 0.25d_0$) for end pins and ($p_1 - 0.5d_0$) for inner upstream pins. The active shear length is equal to the mean value of the gross (Path 2) and the net (Path 1) shear lengths, as defined in Fig. 11.

More recently, Xing et al. [31] pointed out that catenary action contributed to the shear-out resistance of a bolted connection, and proposed Eq. (14).

$$P_{SO,Teh} = 1.2\left(\frac{3d_{pin}}{e_1}\right)^{1/5} L_{av} t f_u \tag{14}$$

Note that in the present study, for the CDL specimens failing in shear-out at the upstream pin hole, there was no free edge downstream of the hole that would enable the catenary action to develop, and thus Eq. (13) is employed.

3.4.2 Bearing resistance ($P_{B,Teh}$)

Teh and Uz [29] adopted the most commonly used format for the bearing resistance equation and employed a bearing coefficient of 3.5, which is greater than the values specified in the current steel and aluminium alloy design codes (ranging from 2.0 to 3.2). The design equation is given by Eq. (15).

$$P_{B,Teh} = 3.5 d_{pin} t f_u \tag{15}$$

For two-pin connections in which the fasteners are oriented in series (such as the CDL specimens) failing in combined bearing and shear-out, the resistance $P_{B\&SO,Teh}$ is computed using Eq. (16a), where a reduction factor equal to min [$L_{av}/(3d_{pin})$, 1] [29] accounts for the fact that the ultimate limit states of bearing and shear-out of the two holes do not occur simultaneously.

$$P_{B\&SO,Teh} = \left(L_{av} / 3d_{pin}\right) P_{SO,Teh} + P_{B,Teh}, \text{ but } L_{av} / 3d_{pin} \leq 1 \tag{16a}$$

The pitches p_1 of the first three CDL specimens tested in the present work were less than the threshold value between shear-out and bearing failures, equal to 3.42 times the pin diameter or 33 mm, so their upstream pin holes failed in shear-out, as evident from Fig. 7. However, as discussed in the previous section for Specimen CS-61-30-50, the end distance e_1 of each CDL specimen (i.e. 30 mm) was very close to the threshold value of 30.6 mm, i.e. 3.11 versus 3.17 times the pin diameter. The shear-out resistance of the first three CDL specimens was therefore computed using Eq. (16b),

$$P_{SO\&SO,Teh} = \left(L_{av} / 3d_{pin}\right) P_{SO,Teh} + P_{SO,Teh} \tag{16b}$$

in which the first resistance term is for the upstream hole.

3.4.3 Net section tension resistance ($P_{NS,Teh}$)

Teh and Gilbert [28] employed in-plane shear lag factors in calculating the net section tension resistance of a bolted (or pinned) connection, as given by Eq. (17a) for a single pinned connection or a connection with pins in series and by Eq. (17b) for a connection with more than one pin in the considered section (i.e. a connection with pins in parallel):

$$P_{\mathrm{NS,Teh}} = A_{\mathrm{n}} f_{\mathrm{u}} \left(0.9 + 0.1 d_{\mathrm{pin}} / W\right) \quad (17a)$$

$$P_{\mathrm{NS,Teh}} = f_{\mathrm{u}} \left[\sum A_{\mathrm{nt}} \left(0.9 + 0.1 d_{\mathrm{pin}} / p_2\right) + 2 A_{\mathrm{no}} \left(0.9 + 0.05 d_{\mathrm{pin}} / e_2\right)\right] \quad (17b)$$

In Eq. (17), W is the width of the plate, A_{nt} is the net section area between the pin holes, and A_{no} is the net section area flanking the pin row on either side, which is equal to the product of $(e_2 - d_{pin}/2)$ and t.

3.4.4 Block shear resistance ($P_{BS,Teh}$)

Teh and Deierlein [32] proposed an equation for determining the block shear resistance of bolted connections based on the effective shear failure plane. The equation, given by Eq. (18), is included in the 2020 edition of the Aluminium Design Manual.

$$P_{\mathrm{BS,Teh}} = f_{\mathrm{u}} A_{\mathrm{nt}} + 0.6 f_{\mathrm{u}} A_{\mathrm{ev}} \quad (18)$$

in which A_{ev} is the effective shear area equal to the mean value of the gross shear area and the net shear area, i.e. $(A_{gv} + A_{nv})/2$.

3.4.5 Summary of predictions of equations proposed by Teh and co-workers

The design equations proposed by Teh et al. [28-32] generally provide more accurate resistance predictions than the code equations, as shown in Fig. 12 where the test ultimate resistances are plotted against those predicted using different design methods. Specifically, as indicated in Table 3, the design equations proposed by Teh et al. [28-32] offer an average enhancement in design accuracy (and resistance) of over 30%. The predicted failure modes shown in Table 4 also consistently matched the experimental observations.

However, the proposed shear-out equation (Eq. (13)) yielded a very conservative prediction for the specimen with the shortest end distance of 10 mm (CS-61-10-50), despite accounting for the catenary effect [31]. This could be due to the influence of friction, which would be more prominent in this specimen than others because of its lower failure load i.e. the friction force, which is expected to be approximately constant (per pin) between specimens owing to the controlled manner in which the preload is applied, is a higher proportion of the specimen failure load. Similarly, though to a lesser extent, conservative predictions were also obtained for the specimens with the relatively short end distance of 15 mm (CS-61-15-50, CS-63-15-50, CS-82-15-50, CS-04-15-50), as indicated in Table 3.

The only predictions on the unsafe side concerned the two specimens made of high strength aluminium alloy 7A04-T6 – specimens CS-04-15-50 and CS-04-40-50 – which failed in shear-out and bearing, respectively. The present test results are consistent with the finding of Teh and Uz [43] that material ductility has a significant effect on the bearing resistance, as the 7A04-T6 alloy had the least ductility.

Overall, the design proposals of Teh et al. [28-32] offer more accurate predictions of both the resistance and failure mode of the studied aluminium alloy connections compared to existing design provisions and are thus recommended for inclusion in future revisions of design codes; however, there remains scope for improved accuracy and consistency by accounting for the friction contribution generated by preloaded swage-locking pins.

4. Conclusions

An experimental investigation into the structural behaviour of swage-locking pinned aluminium alloy double-shear connections has been presented in this paper. Twenty three swage-locking pinned double-shear connections in four different aluminium alloys, with three different pin configurations and various geometric variables were tested. Four failure modes − shear-out, bearing, net section and block shear − were observed in the tests.

The design equations specified in AA 2015, AS/NZS 1664.1:1997 and EC9 were found to provide unduly conservative predictions of the resistances of the aluminium alloy shear connections, while the proposals by Teh and co-workers were shown to yield much more accurate resistance predictions. Importantly, the latter consistently predicted the correct failure modes, as observed in the tests, while the code equations often predicted incorrect failure modes, as shown in Table 4.

However, all the existing design methods fail to consider explicitly the influence of material ductility, strain-hardening and friction on the resistances of aluminium alloy connections. The findings of this study highlight the need for developing more comprehensive and accurate design rules for swage-locking pinned aluminium alloy double-shear connections on the basis of further experimental and numerical studies, in which the influence of the key parameters can be assessed more broadly.

Acknowledgements

The authors would like to acknowledge the financial support provided by the National Natural Science Foundation of China (Grant No. 51878377). The authors would also like to thank Mr. Yuanwen Ouyang, the chief executive officer of Shanghai Tongzheng Aluminium Engineering Co., Ltd, for the supply of swage-locking pins and the hydraulic rivet gun used in the present work. The authors thank Wen Yan, Ying Yu and Wentao Liu for their assistance in the testing program. The support from the Key Laboratory of Civil Engineering Safety and Durability of the China Education Ministry at Tsinghua University is also highly acknowledged. The first author would also like to thank the China Scholarship Council (CSC) for providing the financial support for his stay at Imperial College London.

References

[1] Wang, Z. X., Wang, Y. Q., Sojeong, J., and Ouyang, Y. W. "Experimental investigation and parametric analysis on overall buckling behaviour of large-section aluminium alloy columns under axial compression." *Thin-Walled Structures,* 2018, 122, 585–596.

[2] Liu, X. C. "Research on the mechanical behaviour of TEMCOR joints used in aluminium alloy grid structures." 2016, Master thesis, Tsinghua University, Beijing. (in Chinese)

[3] Das, S. K., and Kaufman, J. G. *Aluminium alloys for bridges and bridge decks*. The Minerals, Metals & Materials Society, Warrendale, PA, 2007, 61–72.

[4] Su, M. N., Young, B., and Gardner, L. "Deformation-based design of aluminium alloy beams. *Engineering Structures*, 2014, 80, 339–349.

[5] Mazzolani, F. M., and Piluso, V. "Prediction of the rotation capacity of aluminium alloy beams." *Thin-Walled Structures,* 1997, 27(1), 103–116.

[6] Su, M. N., Young, B., and Gardner, L. "Testing and design of aluminium alloy cross sections in compression." *Journal of Structural Engineering*, 2014, 140(9), 04014047.

[7] Wang, Y. Q., Wang, Z. X., Hu, X. G., Han, J. K., and Xing, H. J. "Experimental study and parametric analysis on the stability behaviour of 7A04 high-strength aluminium alloy angle columns under axial compression." *Thin-Walled Structures*, 2016, 108, 305–320.

[8] Zhu, J. H., and Young, B. "Aluminium alloy circular hollow section beam-columns." *Thin-Walled Structures*, 2006, 44(2), 131–140.

[9] Zhao, Y. Z., Zhai, X. M., and Sun, L. J. "Test and design method for the buckling behaviours of 6082-T6 aluminium alloy columns with box-type and L-type sections under eccentric compression." *Thin-Walled Structures*, 2016, 100, 62–80.

[10] Menzemer, C. C., Ortiz-Morgado, R., Iascone, R., and Srivatsan, T. S. "An investigation of the bearing strength of three aluminium alloys." *Materials Science and Engineering: A*, 2002, 327(2), 203–212.

[11] Tajeuna, T. A., Légeron, F., Labossière, P., Demers, M., and Langlois, S. "Effect of geometrical parameters of aluminium-to-steel bolted connections." *Engineering Structures*, 2015, 102, 344–357.

[12] Cho, Y. H., and Kim, T. S. "Estimation of ultimate strength in single shear bolted connections with aluminium alloys (6061-T6)." *Thin-Walled Structures*, 2016, 101, 43-57.

[13] Hwang, B. K., and Kim, T. S. "An investigation on ultimate strength of high strength aluminium alloys four-bolted connections with out-of-plane deformation." *International Journal of Steel Structures*, 2019, 19(4), 1158–1170.

[14] Wang, Z. X., Wang, Y. Q., Zhang, G. X., and Shi, Y. J. "Tests and parametric analysis of aluminium alloy bolted joints of different material types." *Construction and Building Materials*, 2018, 185, 589–599.

[15] Amerini, F., and Meo, M. “Structural health monitoring of bolted joints using linear and nonlinear acoustic/ultrasound methods.” *Structural Health Monitoring*, 2011, 10(6), 659–672.

[16] Jiang, Y., Zhang, M., and Lee, C. H. “A study of early stage self-loosening of bolted joints.” *Journal of Mechanical Design*, 2003, 125(3), 518–526.

[17] Chen, W. G., Deng, H., Bai, G. B., and Dong, S. L. “Experimental study on shearing behaviour of lockbolted lap connection for aluminium alloy plates” *Journal of Building Structures*, 2016, 37(1), 143–149. (in Chinese)

[18] Chen, W. G., Deng, H., Dong, S. L., and Zhu, Z. Y. “Numerical modelling of lockbolted lap connections for aluminium alloy plates.” *Thin-Walled Structures*, 2018, 130, 1–11.

[19] Shi, Y., Li, J., Zhang, G., Huang, J. K., and Gu, Y. F. “Corrosion behaviour of aluminium-steel weld-brazing joint.” *Journal of Materials Engineering and Performance*, 2016, 25(5), 1916–1923.

[20] Bouchaïr, A., Averseng, J., and Abidelah, A. “Analysis of the behaviour of stainless steel bolted connections.” *Journal of Constructional Steel Research*, 2008, 64(11), 1264–1274.

[21] Wang, J. C., Jin, X., Zheng, B. F., Shu, G. P., and Jiang, Q. L. “Tests of high strength stainless steel bolted connection of slip-critical type.” *Proceedings of the Eighteenth National Academic Seminar on Modern Structural Engineering*, Cang Zhou, China, 2018, 277–281. (in Chinese)

[22] Zhou, L. “Structure analysis study on aluminium alloy dome of Chong Qing Kong Gang Stadium.” 2009, Master thesis, Chongqing University, Chongqing. (in Chinese)

[23] Guo, X. N., Xiong, Z., Luo, Y. F., Qiu, L. Q., and Liu, J. "*Experimental investigation on the semi-rigid behaviour of aluminium alloy gusset joints*." *Thin-Walled Structures,* 2015, 87, 30–40.

[24] Wang, Z. X., Wang, Y. Q., Zhang, Y., Gardner, L., and Ouyang, Y. W. "Experimental investigation and design of extruded aluminium alloy T-stubs connected by swage-locking pins." *Engineering Structures*, 2019, 200, 109675.

[25] AA (Aluminium Association). "Specification for aluminium structures: Aluminium design manual (ADM)." 2015, Washington, DC: Aluminium Association.

[26] Standards Australia. "Aluminium structures part 1: Limit state design." 1997, *AS/NZS 1664.1:1997,* Sydney, Australia.

[27] CEN (European Committee for Standardization). "Eurocode 9: Design of aluminium structures—Part 1-1: General structural rules." 2007, *BS EN 1999-1-1:2007,* Brussels.

[28] Teh, L. H., and Gilbert, B. P. "Net section tension capacity of bolted connections in cold-reduced steel sheets." *Journal of Structural Engineering*, 2012, 138(3), 337–344.

[29] Teh, L. H., and Uz, M. E. "Combined bearing and shear-out capacity of structural steel bolted connections." *Journal of Structural Engineering*, 2016, 142(11), 04016098.

[30] Teh, L. H., and Uz, M. E. "Ultimate shear-out capacities of structural-steel bolted connections." *Journal of Structural Engineering*, 2015, 141(6), 04014152.

[31] Xing, H. Y., Teh, L. H., Jiang, Z. Y., and Ahmed, A. "Shear-out capacity of bolted connections in cold-reduced steel sheets." *Journal of Structural Engineering*, 2020, 146(4), 04020018.

[32] Teh, L. H., and G. G. Deierlein. "Effective shear plane model for tearout and block shear failure of bolted connections." *Engineering Journal AISC*, 2017, 54 (3): 181–194.

[33] ASTM (American Society for Testing and Materials). "Standard test methods for tension testing of metallic materials." 2015, *E8/E8M-15a*, West Conshohocken, USA.

[34] Ramberg, W., and Osgood W. R. Description of stress–strain curves by three parameters. Technical Note No. 902. 1943, Washington, DC: National Advisory Committee for Aeronautics.

[35] Yun, X., Wang, Z. X., and Gardner, L. "Full-range stress-strain curves for aluminum alloys." *Journal of Structural Engineering*, 2021, DOI: 10.1061/(ASCE)ST.1943-541X.0002999. (in press).

[36] Salih, E. L., Gardner, L., and Nethercot, D. A. "Numerical investigation of net section failure in stainless steel bolted connections." *Journal of Constructional Steel Research*, 2010, 66(12), 1455-1466.

[37] Teh, L. H., and Clements, D. D. "Block shear capacity of bolted connections in cold-reduced steel sheets." *Journal of Structural Engineering*, 2012, 138(4), 459–467.

[38] CEN (European Committee for Standardization). "Eurocode 3: Design of steel structures—Part 1-8: Design of joints." 2005, *BS EN 1993-1-8: 2005*, Brussels

[39] American Institute of Steel Construction (AISC). Load and resistance factor design specification for structural steel buildings, 1993, AISC, Chicago.

[40] Standards Australia. "Cold-formed steel structures." 2005, *AS/NZS 4600:2005*, Sydney, Australia.

[41] AISI (American Iron and Steel Institute). “North American specification for the design of cold-formed steel structural members.” 2016, *AISI S100-16*, Washington, DC: AISI.

[42] Standards Australia. “Cold-formed steel structures.” 2018, *AS/NZS 4600:2018*, Sydney, Australia.

[43] Teh, L. H., and Uz, M. E. “Effect of loading direction on the bearing capacity of cold-reduced steel sheets”. *Journal of Structural Engineering*, 2014, 140(12), 06014005.

Tables:

Table 1. Summary of measured material properties of aluminium alloy inner plates of the shear connection test specimens

Material	E (MPa)	$f_{0.2}$ (MPa)	f_u (MPa)	n	$f_u/f_{0.2}$	ε_u (%)	$\varepsilon_{f,el}$ (%)	$\varepsilon_{f,re}$ (%)	$\varepsilon_{f,re}/\varepsilon_{f,el}$
6061-T6	68,100	275	320	23.4	1.17	8.7	17.1	47.5	2.8
6063-T5	68,300	170	225	12.8	1.33	8.2	18.7	100.3	5.4
6082-T6	69,200	335	375	36.8	1.11	10.2	17.8	34.3	1.9
7A04-T6	70,900	545	595	42.3	1.09	8.4	8.72	16.7	1.9

Table 2. Summary of material and geometric properties of test specimens

Type of connection	Specimen	Alloy	e_1 (mm)	e_2 (mm)	p_1 (mm)	p_2 (mm)
Type 1	CS-61-10-50	6061-T6	10	50	–	–
Type 1	CS-61-15-50	6061-T6	15	50	–	–
Type 1	CS-61-20-50	6061-T6	20	50	–	–
Type 1	CS-61-30-50	6061-T6	30	50	–	–
Type 1	CS-61-40-50	6061-T6	40	50	–	–
Type 1	CS-63-15-50	6063-T5	15	50	–	–
Type 1	CS-63-40-50	6063-T5	40	50	–	–
Type 1	CS-82-15-50	6082-T6	15	50	–	–
Type 1	CS-82-40-50	6082-T6	40	50	–	–
Type 1	CS-04-15-50	7A04-T6	15	50	–	–
Type 1	CS-04-40-50	7A04-T6	40	50	–	–
Type 2	CDT-61-30-10-40	6061-T6	30	10	–	40
Type 2	CDT-61-30-15-40	6061-T6	30	15	–	40
Type 2	CDT-61-30-20-40	6061-T6	30	20	–	40
Type 2	CDT-61-30-30-40	6061-T6	30	30	–	40
Type 2	CDT-61-30-40-20	6061-T6	30	40	–	20
Type 2	CDT-61-30-40-25	6061-T6	30	40	–	25
Type 2	CDT-61-30-40-30	6061-T6	30	40	–	30
Type 2	CDT-61-30-40-40	6061-T6	30	40	–	40
Type 3	CDL-61-30-50-20	6061-T6	30	50	20	–
Type 3	CDL-61-30-50-25	6061-T6	30	50	25	–
Type 3	CDL-61-30-50-30	6061-T6	30	50	30	–
Type 3	CDL-61-30-50-40	6061-T6	30	50	40	–

Table 3. Summary of the results from the shear connection tests and comparisons with design resistance predictions

Specimen	Test		Comparisons with design methods			
	P_{Test} (kN)	FM	P_{Test}/P_{AA}	$P_{Test}/P_{AS/NZS}$	P_{Test}/P_{EC9}	P_{Test}/P_{Teh}
CS-61-10-50	20.6	SO	1.61	1.93	2.10	1.47
CS-61-15-50	25.3	SO	1.31	1.58	1.71	1.16
CS-61-20-50	31.2	SO	1.26	1.51	1.59	1.08
CS-61-30-50	41.6	SO	1.68	2.01	1.41	0.99
CS-61-40-50	50.2	B	2.03	2.43	1.62	1.16
CS-63-15-50	19.6	SO	1.46	1.95	1.91	1.30
CS-63-40-50	38.6	B	2.23	2.98	1.79	1.28
CS-82-15-50	26.8	SO	1.20	1.44	1.56	1.06
CS-82-40-50	52.5	B	1.82	2.19	1.46	1.04
CS-04-15-50	34.5	SO	0.97	1.16	1.26	0.86
CS-04-40-50	66.7	B	1.45	1.74	1.16	0.83
CDT-61-30-10-40	54.1	NS	1.09	1.31	2.37	1.16
CDT-61-30-15-40	67.5	NS	1.36	1.64	1.24	1.16
CDT-61-30-20-40	80.4	NS	1.62	1.95	1.36	1.15
CDT-61-30-30-40	81.8	BS	1.65	1.98	1.39	1.02
CDT-61-30-40-20	60.7	BS	1.22	1.47	1.40	1.12
CDT-61-30-40-25	64.4	BS	1.30	1.56	1.29	1.06
CDT-61-30-40-30	73.2	BS	1.48	1.77	1.30	1.09
CDT-61-30-40-40	85.7	BS	1.73	2.08	1.45	1.07
CDL-61-30-50-20	63.4	SO^d/SO^u	1.45	1.74	1.53	1.19
CDL-61-30-50-25	67.5	SO^d/SO^u	1.36	1.64	1.46	1.08
CDL-61-30-50-30	75.5	SO^d/SO^u	1.52	1.83	1.47	1.01
CDL-61-30-50-40	84.5	SO^d/B^u	1.71	2.05	1.40	1.02
Mean			1.50	1.82	1.53	1.10
COV			0.195	0.214	0.187	0.123

Note: FM = failure mode; SO = shear-out; B = bearing failure; NS = net section failure; BS = block shear. [d]Failure mode of downstream pin hole; [u]failure mode of upstream pin hole.

Table 4. Comparisons of failure modes observed in the tests and predicted by design methods

Specimen	Test	Comparisons with design methods			
	FM	FM$_{AA}$	FM$_{AS/NZS}$	FM$_{EC9}$	FM$_{Teh}$
CS-61-10-50	SO	SO	SO	SO	SO
CS-61-15-50	SO	SO	SO	SO	SO
CS-61-20-50	SO	(B)	(B)	SO	SO
CS-61-30-50	SO	(B)	(B)	SO	SO
CS-61-40-50	B	B	B	B	B
CS-63-15-50	SO	SO	SO	SO	SO
CS-63-40-50	B	B	B	B	B
CS-82-15-50	SO	SO	SO	SO	SO
CS-82-40-50	B	B	B	B	B
CS-04-15-50	SO	SO	SO	SO	SO
CS-04-40-50	B	B	B	B	B
CDT-61-30-10-40	NS	(B)	(B)	(SO)	NS
CDT-61-30-15-40	NS	(B)	(B)	(SO)	NS
CDT-61-30-20-40	NS	(B)	(B)	(SO)	NS
CDT-61-30-30-40	BS	(B)	(B)	(SO)	BS
CDT-61-30-40-20	BS	(B)	(B)	BS	BS
CDT-61-30-40-25	BS	(B)	(B)	BS	BS
CDT-61-30-40-30	BS	(B)	(B)	BS	BS
CDT-61-30-40-40	BS	(B)	(B)	(SO)	BS
CDL-61-30-50-20	SO[d]/SO[u]	(B[d])/SO[u]	(B[d])/SO[u]	SO[d]/SO[u]	SO[d]/SO[u]
CDL-61-30-50-25	SO[d] /SO[u]	(B[d])/(B[u])	(B[d])/(B[u])	SO[d] /SO[u]	SO[d]/SO[u]
CDL-61-30-50-30	SO[d] /SO[u]	(B[d])/(B[u])	(B[d])/(B[u])	SO[d] /SO[u]	SO[d]/SO[u]
CDL-61-30-50-40	SO[d] /B[u]	(B[d])/B[u]	(B[d])/B[u]	SO[d] /B[u]	SO[d]/B[u]

Note: FM = failure mode; SO = shear-out; B = bearing failure; NS = net section failure; BS = block shear.
[d]Failure mode of downstream pin hole; [u]failure mode of upstream pin hole.
All incorrect predictions have been put in brackets.

Table 5. Assessment of design methods for each failure mode for AA 2015 and EC9

Specimen	P_{Test}/ $P_{B,AA}$	P_{Test}/ $P_{B,EC9}$	P_{Test}/ $P_{NS,AA}$	P_{Test}/ $P_{NS, EC9}$	P_{Test}/ $P_{BS,AA}$	P_{Test}/ $P_{BS, EC9}$
CS-61-10-50	1.61	2.10	N/A	N/A	N/A	N/A
CS-61-15-50	1.31	1.71	N/A	N/A	N/A	N/A
CS-61-20-50	1.26	1.59	N/A	N/A	N/A	N/A
CS-61-30-50	1.68	1.41	N/A	N/A	N/A	N/A
CS-61-40-50	2.03	1.62	N/A	N/A	N/A	N/A
CS-63-15-50	1.46	1.91	N/A	N/A	N/A	N/A
CS-63-40-50	2.23	1.79	N/A	N/A	N/A	N/A
CS-82-15-50	1.20	1.56	N/A	N/A	N/A	N/A
CS-82-40-50	1.82	1.46	N/A	N/A	N/A	N/A
CS-04-15-50	0.97	1.26	N/A	N/A	N/A	N/A
CS-04-40-50	1.45	1.16	N/A	N/A	N/A	N/A
CDT-61-30-10-40	N/A	N/A	1.08	1.20	N/A	N/A
CDT-61-30-15-40	N/A	N/A	1.08	1.19	N/A	N/A
CDT-61-30-20-40	N/A	N/A	1.06	1.18	N/A	N/A
CDT-61-30-30-40	N/A	N/A	N/A	N/A	1.00	1.18
CDT-61-30-40-20	N/A	N/A	N/A	N/A	1.01	1.40
CDT-61-30-40-25	N/A	N/A	N/A	N/A	0.98	1.29
CDT-61-30-40-30	N/A	N/A	N/A	N/A	1.03	1.30
CDT-61-30-40-40	N/A	N/A	N/A	N/A	1.05	1.24
CDL-61-30-50-20	1.45	1.53	N/A	N/A	N/A	N/A
CDL-61-30-50-25	1.36	1.46	N/A	N/A	N/A	N/A
CDL-61-30-50-30	1.52	1.47	N/A	N/A	N/A	N/A
CDL-61-30-50-40	1.71	1.40	N/A	N/A	N/A	N/A
Mean	1.54	1.56	1.07	1.19	1.02	1.28
COV	0.211	0.155	0.009	0.009	0.025	0.062

Figures:

(a) Rafel Gallery, Shanghai, China

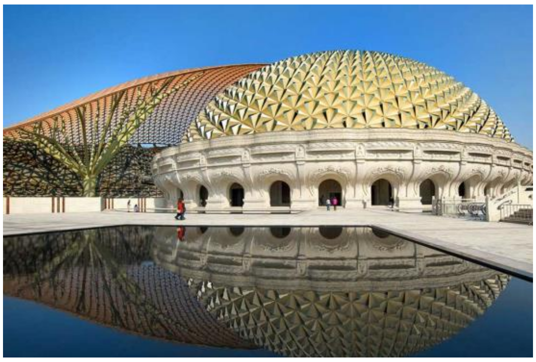

(b) Usnisa Palace, Nanjing, China

(c) Howard Auditorium, Tulsa, USA

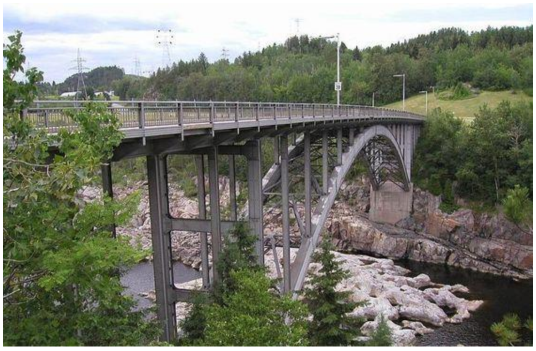

(d) Highway bridge over Saguenay River, Arvida, Canada

Fig. 1. Examples of aluminium alloy structures

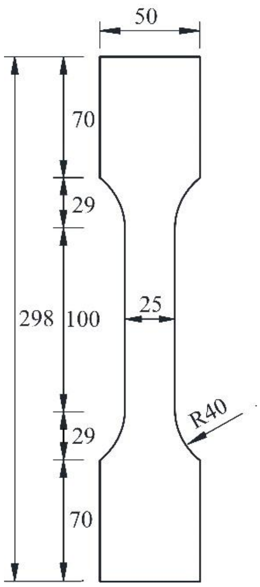

(a) Dimensions of tensile coupons (in mm)

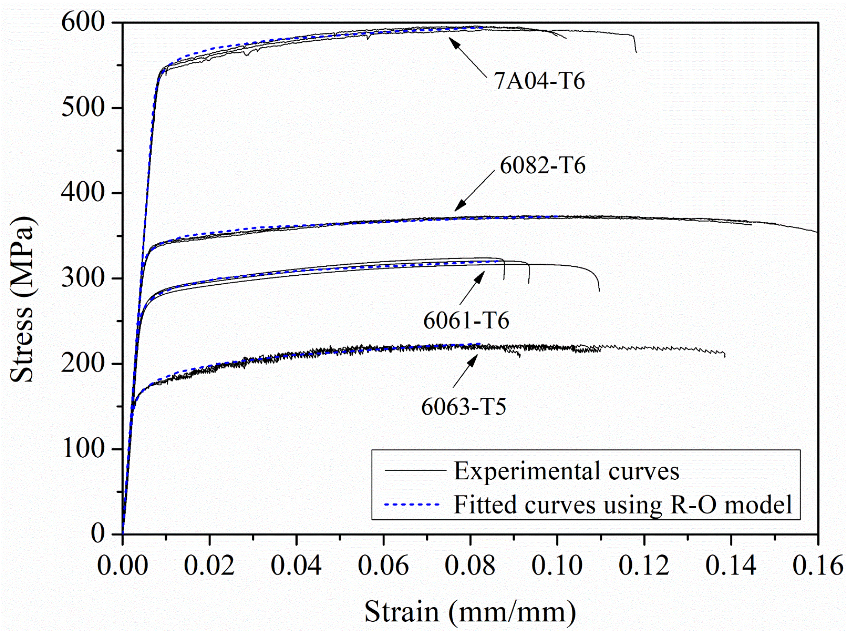

(b) Stress-strain curves

Fig. 2. Dimensions of tensile coupon and stress-strain curves for four investigated aluminium alloys

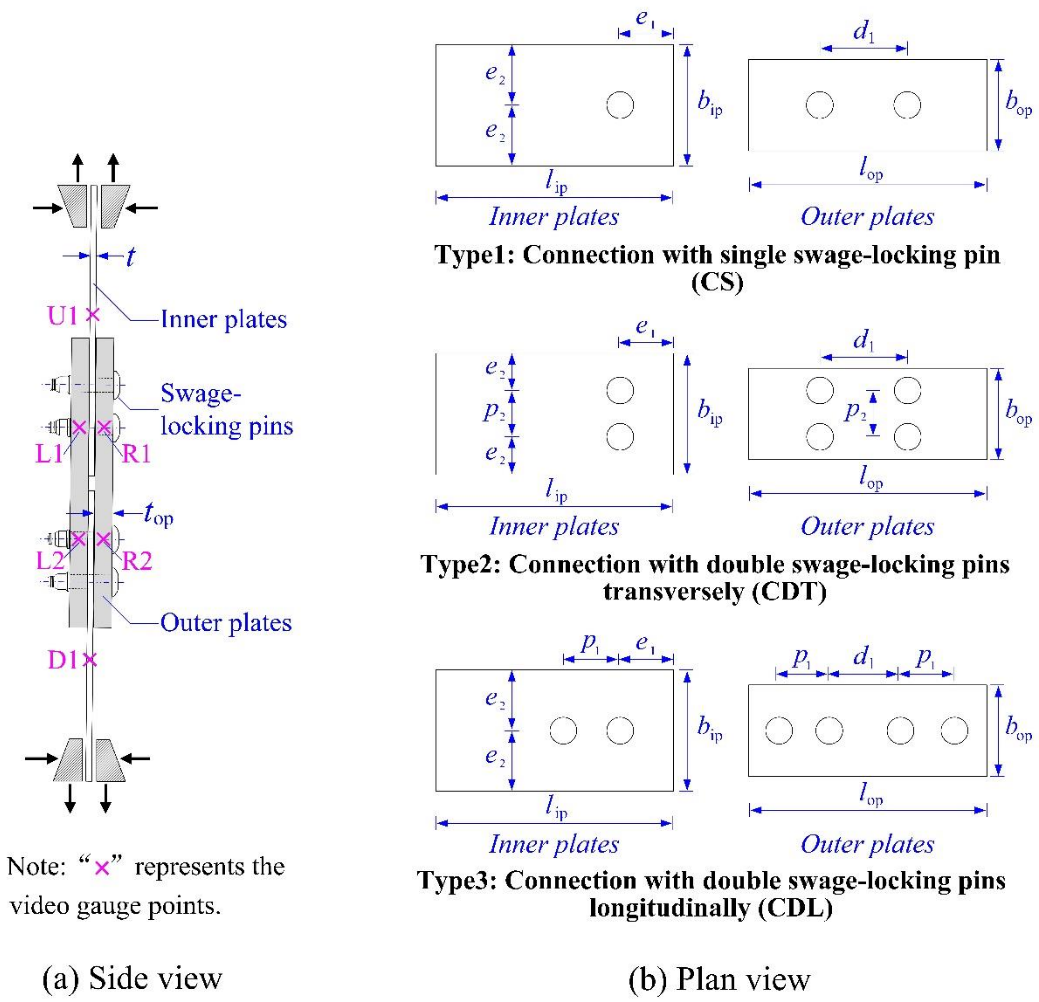

Fig. 3. Configurations of tested shear connections

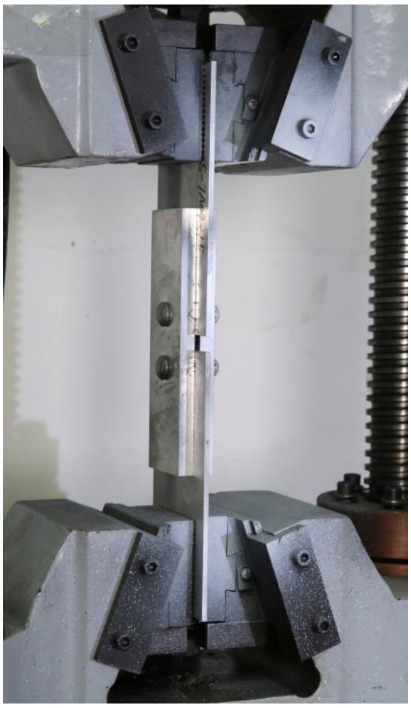

Fig. 4. Experimental setup for shear connection tests

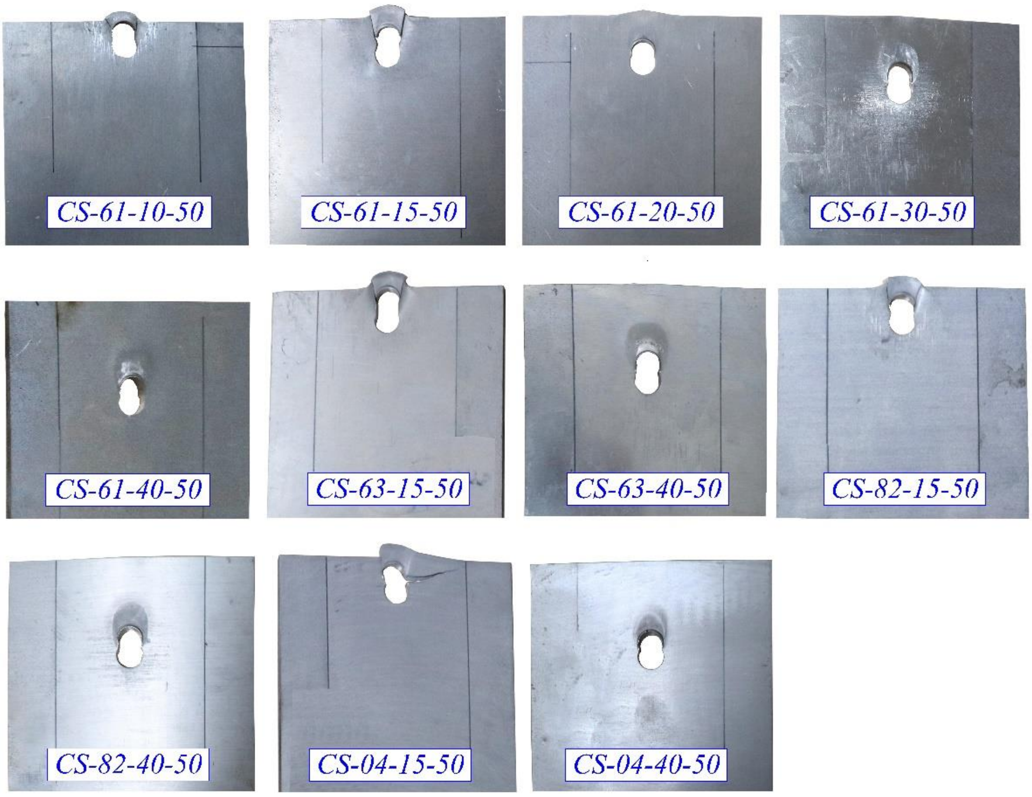

Fig. 5. Failure modes of CS specimens

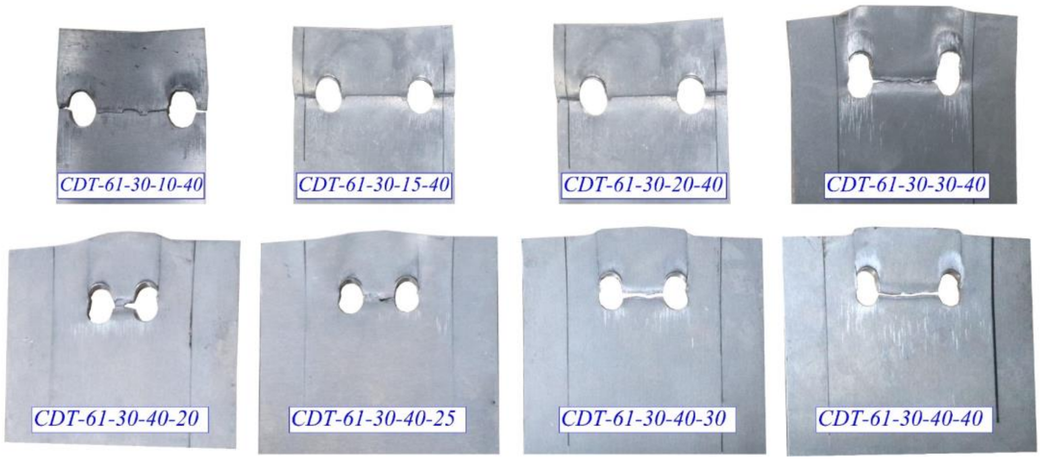

Fig. 6. Failure modes of CDT specimens

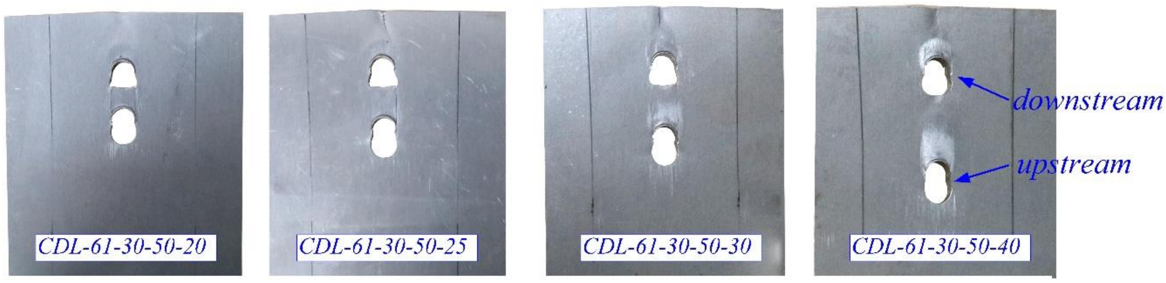

Fig. 7. Failure modes of CDL specimens

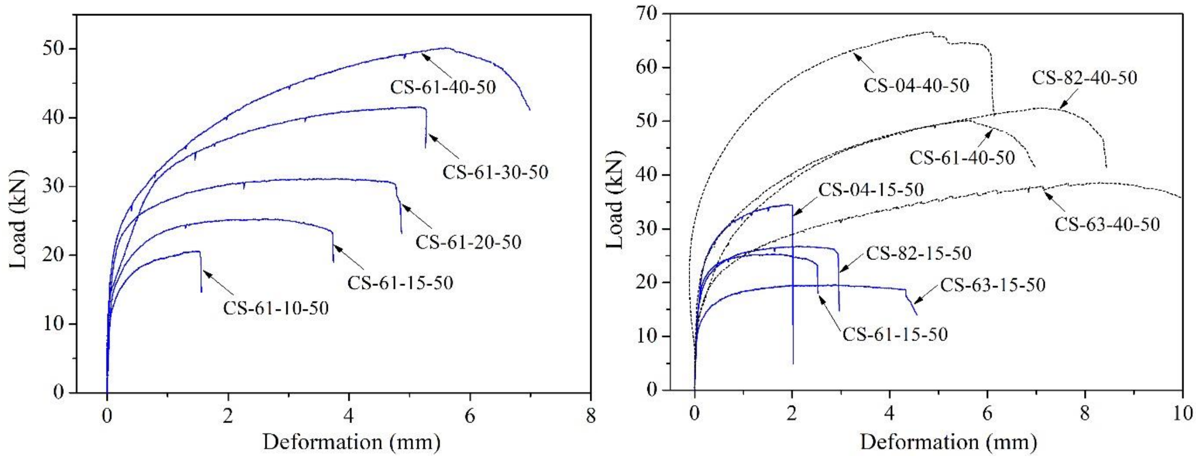

(a) Group to compare the influence of e_1

(b) Group to compare the influence of aluminium alloy grade

Fig. 8. Load-deformation curves of CS specimens

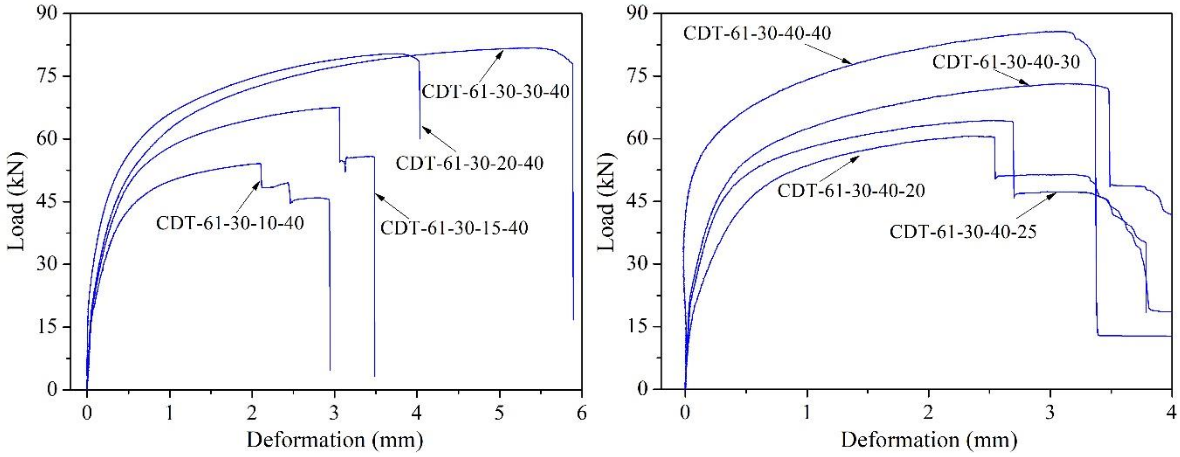

(a) Group to compare the influence of e_2 (b) Group to compare the influence of p_2

Fig. 9. Load- deformation curves of CDT specimens

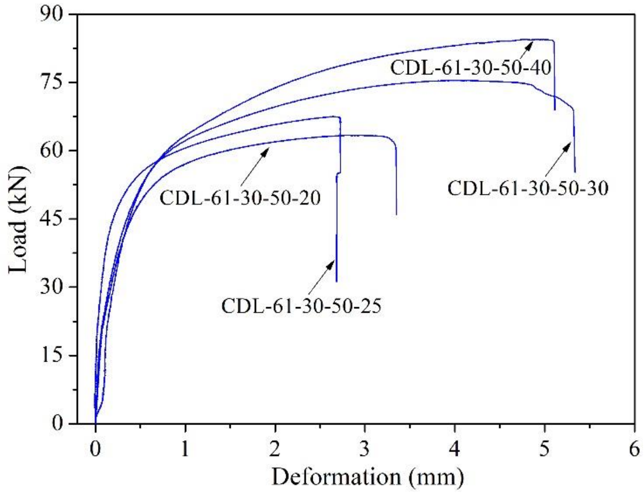

Fig. 10. Load- deformation curves of CDL specimens

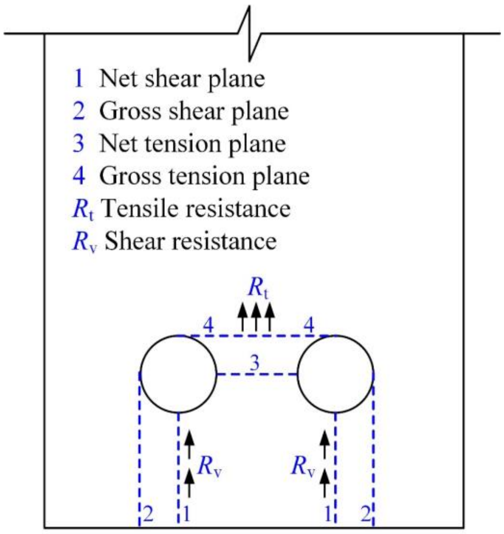

Fig. 11. Geometric variables of block shear resistance

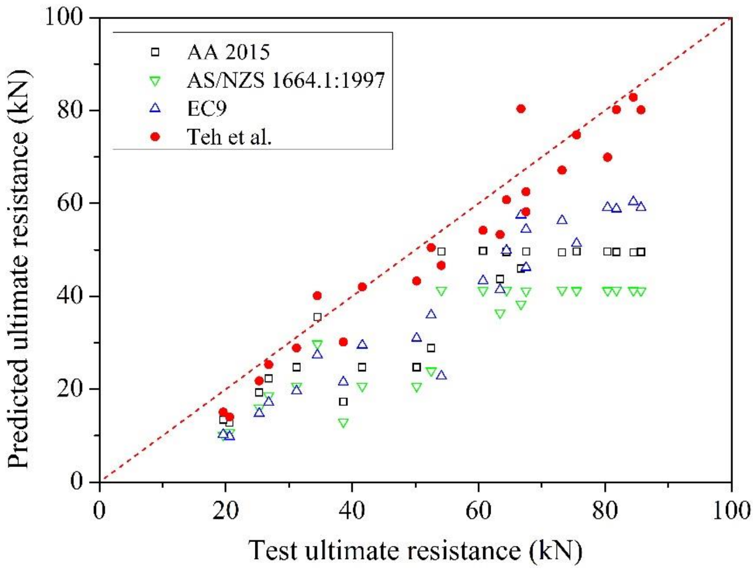

Fig. 12. Comparison between test ultimate resistances and those predicted using different methods